COO-2172-12

RELATIONSHIP BETWEEN ANELASTIC AND NON-LINEAR VISCO-PLASTIC BEHAVIOR OF 316 STAINLESS STEEL AT LOW HOMOLOGOUS TEMPERATURE

N. Nir, F. H. Huang, E. W. Hart* and Che-Yu Li

May, 1976

Department of Materials Science and Engineering

Cornell University, Ithaca, New York 14853

*On leave from General Electric Research & Development Center, Schenectady, New York 12301

DISCLAIMER

ABSTRACT

At low homologous temperature the plastic strain rate seems to be controlled largely by dislocation glide friction. However, since a sizeable fraction of the applied stress σ is dissipated in overcoming the strong barriers due to dislocation tangles generated by strain hardening, only a portion of the applied stress is actually expended against the frictional resistance. A recent model for this process, proposed by Hart,[1] includes the role of dislocation pile-ups at the strong barriers. The pile-ups provide a mechanism for producing the internal back stresses that limit the effective frictional stress. They also appear in the deformation as a stored anelastic strain component. The resultant behavior at low temperature and high stress is similar to that proposed by Gupta and Li.[7] The same model also predicts an anelastic behavior at low stress. Measurements at both high and low stress levels on 316 Stainless Steel have now shown that the predictions of the model are quantitatively consistent at both stress levels.

The experiment reported here was designed to test whether a complete deformation model proposed recently by Hart[1] was fully consistent over its entire predictive range. The consistency test to be described is especially stringent since, according to the model, stress-strain rate measurements in the fully plastic stress range already determine the most important parameters of the model. The model then predicts a low stress anelastic behavior that depends on the same parameters. Consistency requires that the same parameter values yield a reliable description for both fully plastic and anelastic behavior.

The measurements were made on Type 316 Stainless Steel at 25°C. The anelasticity measurements were made by recording strain-time histories after each of a sequence of abrupt load changes, all at stress levels low enough so that no unrecoverable (plastic) straining occurred. These measurements were performed in the same way as those reported earlier by Nir[2] for high-purity Al. The plastic stress-strain rate behavior was measured by load relaxation testing. Such measurements had already been reported for this material by Yamada and Li.[3] However, because of the metallurgical variability of this material, it seemed desirable to repeat the plastic range tests on the same specimen for which the anelasticity measurements had been made. The relationship of the load relaxation test data to the stress-strain rate characteristics has been described in detail elsewhere.[4]

In the following we shall first describe the theoretical model that is under test. The characterization of the experimental specimen will then be described. The experimental results and data analysis will then be presented for the two types of test. Finally

we shall discuss the agreement between the two types of test.

The Deformation Model

The deformation model is described in considerable detail and in three-dimensional context in reference (1). We shall limit our description here to uniaxial deformation for simplicity.

The theory[5] that underlies the model is phenomenological and thus leads directly to deformation constitutive relations. The theory is a state variable theory, and the constitutive equations represent a mechanical plastic equation of state.

The model represents a synthesis of three deformation mechanisms whose mutual relationship is most easily described by the rheological diagram of Fig. 1. The three mechanisms are represented by three elements labeled 1, 2, and 3. We shall refer to them in our discussion by the names a - element (or stored strain element), $\dot{\alpha}$ - element, and $\dot{\epsilon}$ - element (or frictional element) respectively. These elements and their relationships can be taken to represent familiar micro-mechanical processes as was discussed in reference (1). The micro-mechanical relationships are considered to be as follows:

The dislocation flux that is responsible for the non-elastic deformation of the metal grain matrix must traverse not only large regions of relatively well ordered crystal but also the strong barriers to dislocation motion due to dislocation tangles and cell walls. The strong barriers represent the basic strain hardening and are generated by straining. Dislocation motion in the good regions is limited by glide friction. Passage through the strong barriers can occur either by mechanical cutting of dislocations at high enough stress or by thermal activation at lower stresses.

Since the dislocation flux in the good regions will generally exceed the rate of passage of barriers, there will be an accumulation of dislocations in pile-ups at the barriers. The pile-ups will generally raise the driving force for barrier passage and will generate back stresses that slow down the dislocation flux through good crystal.

In our model the $\dot{\alpha}$-element represents the barrier processes, the a-element characterizes the pile-ups as a stored strain, and the $\dot{\varepsilon}$-element represents the glide friction. The resultant mechanical interactions among the processes and the dislocation flux balance is then accounted for by the diagram of Fig. 1. These relations will now be described quantitatively.

The applied uniaxial stress σ is the sum of the stresses σ_a and σ_f that are operative in each branch of the diagram. The observed total inelastic uniaxial strain rate $\dot{\varepsilon}$ is the same as the strain rate exhibited by the lower branch and is equal to the sum of the strain rate component $\dot{\alpha}$ and the time rate of change of stored strain a. Thus we have two constraint equations on the auxiliary variables σ_a, σ_f, $\dot{\alpha}$, and a. These are

$$\sigma = \sigma_a + \sigma_f \ , \tag{1}$$

$$\dot{\varepsilon} = \dot{\alpha} + da/dt \ . \tag{2}$$

The constitutive equations for the component elements are as follows:

The a-element is a linear elastic element with a modulus M such that

$$\sigma_a = Ma \ . \tag{3}$$

The $\dot{\alpha}$-element is the plastic-creep element satisfying the relations

$$\ln(\sigma^*/\sigma_a) = (\dot{\varepsilon}^*/\dot{\alpha})^{\lambda} \quad , \tag{4}$$

$$\dot{\varepsilon}^* \equiv (\sigma^*/G)^{m_f} e^{-(Q/RT)} \quad , \tag{5}$$

$$d\ln\sigma^*/dt = \Gamma(\sigma_a,\sigma^*)\dot{\alpha} - R(\sigma^*,T) \quad . \tag{6}$$

In these equations T is the absolute temperature, R is the gas constant, G is the modulus of rigidity at temperature T, and λ, f, m, and Q are constants for each material. The functions Γ and R are to be determined experimentally.

The $\dot{\alpha}$-element depends prominently on the scalar state variable σ^* which we shall call the hardness. The strain hardening is then conveniently represented by an evolution equation that provides for incremental increase of hardness with strain increments $d\alpha$ and for purely thermal recovery of hardness. In the tests described here, the recovery term R is entirely negligible. The structure of Γ is described in greater detail elsewhere[1,6] and is not important in the current paper. The dependence of $\dot{\alpha}$ on σ_a will be described below graphically and will be shown to be especially simple for the experiment under discussion.

Finally, the $\dot{\varepsilon}$-element, which represents dislocation glide friction, can be represented over fairly large ranges of strain rate $\dot{\varepsilon}$ as a non-linear viscous element with a power law behavior. In order to emphasize that $\dot{\varepsilon}$ has the same sign as σ_f we write this relation with the signum function (sgn) whose value is simply the algebraic sign of the argument. Thus

$$\dot{\varepsilon} = \dot{a}^*(T)(|\sigma_f|/M)^M \mathrm{sgn}(\sigma_f) \quad . \tag{7}$$

We omit the signum and absolute value sign below when both $\dot{\varepsilon}$ and σ_f are positive. The rate variable $\dot{a}^*$ is to be measured as a function of temperature. For our isothermal experiment it is of course a

constant. The exponent M is a constant for any one material if such a simple power law is obeyed. This representation will be adequate for our experiment.

Some typical values of the material constants are: $N \cong 7\text{-}9$, $m \cong 4\text{-}5$, $\lambda \approx 0.15$, M is of the order of G, and Q is commonly the same as the activation energy for self-diffusion of the atomic species.

Application of the Model

If a specimen, for which the initial value of α is zero, is loaded at an applied stress σ, the strain rate $\dot{\epsilon}$ is initially high, and it rapidly decreases to a lower more steady value. There then ensues a further much slower time rate of decrease of $\dot{\epsilon}$. The initial loading transient corresponds to a rapid increase in the value of α until the time when $d\alpha/dt$ falls to a level much lower than $\dot{\epsilon}$. The subsequent slower rate of reduction of $\dot{\epsilon}$ is due principally to the continued strain hardening of the $\dot{\alpha}$-element. Now, in the transient-free stage, $\dot{\alpha}$ is closely equal to $\dot{\epsilon}$ and so we can plot both σ_a and σ_f against $\dot{\epsilon}$. This is done schematically in Fig. 2 for a fixed value of σ^*, and for a typically low homologous temperature case. The curve of operative applied stress σ is shown as the sum of σ_a and σ_f, and in such a temperature range it is typically concave upward as a function of $\dot{\epsilon}$. The σ_a curve as shown becomes asymptotically tangent to the line $\sigma=\sigma^*$ at large $\dot{\epsilon}$ and so at sufficiently low temperature σ^* appears substantially as a plastic yield stress for the $\dot{\alpha}$-element. This is in fact the situation for the 316 Stainless Steel of the current experiment.

We may then employ a considerably simplified version of our

equation of state for the transient free behavior as follows:

$$da/dt = 0 \ , \tag{8}$$

and so

$$\dot{\alpha} = \dot{\epsilon} \ . \tag{9}$$

Now to a very good approximation

$$\sigma_a = \sigma^* \ , \tag{10}$$

and so

$$\sigma_f = \sigma - \sigma^* \ . \tag{11}$$

Then $\dot{\epsilon}$ can be obtained directly from Equation (7) as

$$\dot{\epsilon} = \dot{a}^* [(\sigma - \sigma^*)/M]^M \ . \tag{12}$$

This equation can be rewritten in the form

$$\dot{\epsilon} = \dot{a}^* (\sigma^*/M)^M \ [(\sigma/\sigma^*) - 1]^M \ . \tag{13}$$

Then, if σ is scaled by σ^*, and $\dot{\epsilon}$ by $(\sigma^*/M)^M$, the resultant scaled $\dot{\epsilon}$ vs σ curve is a single invariant curve. This means that a set of transient-free $\ln\sigma$ vs $\ln\dot{\epsilon}$ curves at a variety of values of σ^* can be made to superpose exactly by translation along a fixed direction with slope 1/M. Such a behavior had already been reported by Yamada and Li[3] for the material under discussion, and we show a set of such curves obtained in the present experiment in Fig. 3.

The important thing about the scaling behavior is that it provides an experimental determination of the exponent M from the scaling direction independently of the shape of the curves.

Now the same theory that describes the transient-free behavior also makes a unique prediction of the transient behavior. The transient, at low homologous temperature, is most sensitively measured at low σ since the relaxation time for the transient is then much longer than at a high stress level. Furthermore, if σ is much

smaller than σ^*, $\dot{a}$ is entirely negligible and the $\dot{\alpha}$-element is effectively frozen. The model then appears simply as an anelastic body with Hookean spring but with non-Newtonian dash-pot. In this range $\dot{\alpha}=0$ and

$$\dot{\epsilon} = da/dt \ . \qquad (14)$$

The resultant constitutive equation for this behavior (writing $\dot{a}$ for da/dt) is

$$\dot{a} = \dot{a}^* \ [(\sigma - \sigma_a)/M]^M \ . \qquad (15)$$

Now application of Equation (3) leads to the equation

$$\dot{a} = \dot{a}^* \ [(\sigma/M) - a]^M \ , \qquad (16)$$

or if we introduce the saturation anelastic strain a^S for σ/M this can be written

$$\dot{a} = \dot{a}^* \ [a^S - a]^M \ . \qquad (17)$$

The Consistency Test

We have deduced from a single model the behavior of the deformation at low homologous temperature both in the fully plastic range for which $\sigma>\sigma^*$ and in the anelastic range for which $\sigma<<\sigma^*$. The predictions for the former case are given simply by Equations (12) and (13) and in the latter case by Equations (16) and (17). Tests of either case will completely determine the material constants M and $\dot{a}^*$ if M is known, and M is determined by the anelasticity tests. A crucial test of consistency, then, is the extent of agreement of the values of M and $\dot{a}^*$ determined by the two types of measurement.

Tests are reported in the following for both high and low σ behavior for 316 Stainless Steel. The consistency of the predictions will be shown to be quite good.

In the anelasticity measurements it will be shown that in addition to the grain matrix anelasticity discussed above there is also a readily identifiable linear anelasticity due to grain boundary sliding. The same behavior was found and described in the earlier work on high-purity aluminum.[2] This component is unimportant in the plastic range measurements since grain boundary sliding plays no significant role in plastic deformation at low temperature. The test of the theory concerns only the grain matrix behavior. To distinguish the quantities for grain boundary anelasticity from those for grain matrix anelasticity we shall use subscripts gb and m for the two cases respectively as was done in reference (2). Thus, in the following, Equations (16) and (17) will simply be rewritten with the m subscript throughout.

The Experimental Procedure

The 316 Stainless Steel used in this experiment was a commercial grade obtained from Allegheny Ludlum Steel Co. The gage section of the single specimen was 1.0 inch long with a diameter of 0.1 inch. After machining, the specimen was annealed in vacuum for five minutes at 1200°C and air cooled. It was then strained 5% at room temperature in tension and annealed in Argon at 800°C for 48 hours. The average grain size was then 45μm. The specimen was then prestrained 20% in tension prior to the start of the load change measurements.

The principles and the procedures for the anelastic deformation (load change) experiment and for the load relaxation experiment have been described in references (2) and (4).

As mentioned above, the stress level during the load change tests was always so low that the plastic (unrecoverable) strain

rate was negligible. After each abrupt load change the specimen extension was measured as a function of time.

The load relaxation tests yielded records of load vs. time. From that data the plastic strain rate $\dot{\varepsilon}$ could be determined as a function of stress for each relaxation run.

The load relaxation tests were performed on the same specimen after the anelasticity measurements were concluded.

The Plastic Range Load Relaxation Tests

The load relaxation results in the form of curves of $\log\sigma$ vs. $\log\dot{\varepsilon}$ are shown in Fig. 3. These data were obtained from the same specimen on which the anelasticity measurements had been made. The curves shown represent three different levels of hardness. The different hardness levels were obtained by about 1% interim plastic straining between each pair of relaxation runs.

These data are consistent with those reported by Yamada and Li.[3] The constant hardness curves are of the same shape and they exhibit the same σ-$\dot{\varepsilon}$ scaling behavior. The curves in Fig. 3 can be superposed by translation along the line shown in the figure. The slope of that line, according to Equation (13) is $1/M$. The value of the exponent obtained this way is 7.7 ± 0.2. Since the range of hardness of the curves in Fig. 3 is so small, the accuracy of determination of M is not very sharp by this means. A sharper determination of M is obtained by fitting the actual shape of the curves according to Equation (13). By that means M is found to be 7.8 ± 0.1.

The solid lines through the data points in Fig. 3 are plots of Equation (13) with M = 7.8 and the parameter values shown in Table I. The value of $\hat{\sigma}_m$ has been taken to be 1.01×10^5 MN/m^2 as

determined in the anelasticity analysis below, and $\dot{a}^* = 1.65 \times 10^{21}$ sec^{-1}.

THE ANELASTICITY TESTS

Two distinct components, similar to those found in aluminum,[2] were observed for the anelastic strain. One component had a very short time constant and is associated with the grain boundary. The other component saturated over a much longer time period and is associated with the grain matrix. These two components can be identified easily from the data shown in Fig. 4 in which the logarithm of the anelastic strain rate is plotted against the difference between the saturation and the current anelastic strain.

The Grain Boundary Anelasticity

The grain boundary anelastic strain a_{gb} was found to satisfy a linear relaxation equation of the form

$$\dot{a}_{gb} = \dot{a}^*_{gb} \, (a^s_{gb} - a_{gb}) \, , \qquad (18)$$

where $\dot{a}^*_{gb}$ is a rate constant and a^s_{gb} is the saturation grain boundary anelastic strain at stress σ. A linear relationship was found for a^s_{gb} of the form

$$a^s_{gb} = \sigma / M_{gb} \, , \qquad (19)$$

and M_{gb} is a grain boundary anelastic modulus.

Integration of Equation (18) with respect to time t and substitution into Equation (18) (see ref. 2) yields the relationship

$$\ln \dot{a}_{gb} = \ln[\dot{a}^*_{gb}(a^s_{gb} - a^o_{gb})] - \dot{a}^*_{gb} t \, , \qquad (20)$$

where a^o_{gb} is the anelastic strain at time t=o. The initial anelastic strain a^o_{gb} at the time of a load change is generally the saturation anelastic strain at the prior load.

A plot of $\ln\dot{a}_{gb}$ vs. t is shown in Fig. 5 for the data of two separate test runs. The data agree well with the relation of Equation (20). From the data the average parameter values determined were $\dot{a}^*_{gb} = 12.1\pm1.1\ sec^{-1}$ and $M_{gb} = 1.69\pm0.12\times10^7$ psi ($1.16\pm0.08\times10^5 MN/m^2$). The individual determinations for each run are shown in Table II.

The Grain Matrix Anelasticity

The long time anelasticity data of Fig. 4 is the grain matrix anelastic strain a_m. The non-linear relation of Equation (17) was found to provide a good fit for the observed data.

Integration of Equation (17) yields

$$(a^s_m - a^o_m)^{1-M} - (a^s_m - a_m)^{1-M} = (1-M)\dot{a}^*_m(t-t_o) \quad , \qquad (21)$$

where a^o_m is the grain matrix anelastic strain at time $t=t_o$. This equation was used to analyze the grain matrix anelastic strain by means of a non-linear least squares fitting routine. The best fit curves to two of the test runs are shown plotted with the data points in Fig. 6.

The average values of the best parameters determined individually from four runs are: $M = 7.7\pm0.2$, $\dot{a}^*_m = 7.0\pm2.0\times10^{20} sec^{-1}$, and $M_m = 1.46\pm0.07\times10^7$psi ($1.01\pm0.05\times10^5 MN/m^2$). The separate individual determinations are listed in Table III.

More pertinent for the current experiment is the value of $\dot{a}^*_m$ obtained with a single value of M for all runs. These are also shown in Table III for the single "best" value M = 7.8. For that case the geometric mean value of $\dot{a}^*_m$ is $1.14\times10^{21} sec^{-1}$. This value is uncertain to within a factor of about 2.5.

DISCUSSION OF RESULTS

In order to test the model described above, tests were made on 316 Stainless Steel of two levels of stress that differed by a factor of about thirty. The material was fully plastic at the upper stress level and was entirely anelastic at the lower stress level.

The principal feature of the model that was under test was the $\dot{\epsilon}$-element. This non-linear frictional term is characterized by the rate constant $\dot{a}_m^*$ and a stress exponent M. Both ranges of data were fit quite well over a broad range of strain rate with M = 7.8. The best values of $\dot{a}_m^*$ were $1.65 \times 10^{21} sec^{-1}$ for the high stress data and 1.14×10^{21} for the low stress data. These agree quite well within the experimental uncertainty.

The interpretation of the high stress data offered by our model is very similar to that made by Gupta and Li[7] with respect to low homologous temperature tests of several bcc metals and alloys. Gupta and Li characterized the results of their load relaxation tests substantially as we have done in Equation (12) above. What we have called σ_a in our model is equivalent to the internal stress σ_i in their treatment. Furthermore, both treatments associate the principal effective flow stress (our σ_f) with dislocation glide resistance.

Our model goes beyond that of Gupta and Li in providing a mechanism whereby the essentially dissipative strain hardening barrier stress σ^* is reflected as dislocation pile-up back stress σ_a operating directly on the gliding dislocations. A corollary of our model is then the low stress anelastic behavior.

Because of the considerably greater range of strain rate ex-

plored in our experiment, the test of the model could be more stringent.

Thus our results are not only consistent with the Gupta and Li treatment but also provide support for a more detailed model.

Although a power law seems to hold well over a broad strain rate range at a single temperature, we have no confidence in the universality of such a representation. Measurements of $\dot{a}_m^*$ and M at other temperatures are necessary to settle this question. Such investigations are in fact now in progress.

ACKNOWLEDGEMENT

This work is supported by the National Science Foundation and the Energy Research and Development Administration.

TABLE I

Best Fit Parameters for
Stress-Strain Rate Curves of Figure 3

Curve Number	Accumulated Tensile Strain (per cent)	σ^* (MN/m^2)
1	20.75	637.8
2	21.49	646.4
3	22.69	660.0

$M = 7.8$; $M_m = 1.01 \times 10^5 MN/m^2$; $\dot{a}^* = 1.65 \times 10^{21} sec^{-1}$

TABLE II

Experimental Data and Values of the Calculated Grain Boundary Anelastic Parameters.

σ Initial Stress MN/m^2	$\Delta\sigma$ MN/m^2	Δa^s_{gb}	M_{gb} MN/m^2	$\dot{a}^*_{gb}$ sec^{-1}
8.78	34.58	30.83×10^{-5}	1.42×10^{5}	13.25
43.36	-34.54	27.52×10^{-5}	1.25×10^{5}	11.00
21.08	17.32	15.92×10^{-5}	1.08×10^{5}	11.10
38.4	-17.24	14.30×10^{-5}	1.21×10^{5}	11.95

TABLE III

Experimental Data and Values of the Calculated Grain Matrix Anelastic Parameters

σ Initial Stress MN/m^2	$\Delta\sigma$ MN/m^2	Δa^s_m	M_m MN/m^2	$\dot{a}^*_m$ sec^{-1}	M	$\dot{a}^*_m$ for M=7.8 sec^{-1}
8.78	34.58	35.5×10^{-5}	0.97×10^{5}	5.4×10^{20}	7.86	3.7×10^{20}
43.36	-34.54	33.5×10^{-5}	1.03×10^{5}	9.68×10^{20}	7.69	1.9×10^{21}
21.08	17.32	18.0×10^{-5}	0.96×10^{5}	5.1×10^{20}	7.80	5.1×10^{20}
38.4	-17.24	16.0×10^{-5}	1.07×10^{5}	7.4×10^{20}	7.51	4.7×10^{21}

REFERENCES

1. E. W. Hart, ASME Trans. J. of Eng. Mtl. & Tech., 1976, in press.
2. N. Nir, E. W. Hart and C-Y. Li, Scripta Met., 1976, vol. 10, p. 189.
3. H. Yamada and C-Y Li, Met. Trans. 1974, vol. 22, p. 249.
4. D. Y. Lee and E. W. Hart, Met. Trans. 1971, vol. 2, p. 1245.
5. E. W. Hart, Acta Met., 1970, vol. 18, p. 599.
6. E. W. Hart, C-Y. Li, H. Yamada and G. L. Wire, "Constitutive Equations in Plasticity," Edited by A. Argon (1975, MIT Press).
7. I. Gupta and J. C. M. Li, Met. Trans., 1970, vol. 1, p. 2323.

FIGURE CAPTIONS

Figure 1: A schematic rheological diagram representing Hart's model[1] of the constitutive relations for metal grain matrix non-elastic flow. Element 1 is Hookean, element 2 is a thermal activation element associated with plastic deformation and element 3 is a non-linear viscous element.

Figure 2: A schematic graph of stress vs. strain rate for transient-free flow at low homologous temperature. The observed flow stress σ, as shown by the upper curve, is the sum of stresses represented by the two lower curves, of σ_a and σ_f.

Figure 3: $\log_{10}\sigma$ vs. $\log_{10}\dot{\epsilon}$ data obtained from room temperature load relaxation experiments at several plastic strain levels. The curves are calculated by using Equations 1-4 and 7, with the parameters in Table I.

Figure 4: Logarithm of the magnitude of the anelastic strain rate plotted against the difference between the saturation and current anelastic strain. The time shown is the elapsed time after the stress change. The value of (a^s-a) decreases with increasing time. The value of a^s in this figure is the sum of the saturation anelastic strains of the grain boundary and the grain matrix, and it is calculated from the two anelastic moduli.

Figure 5: Logarithm of the magnitude of the grain boundary anelastic strain rate plotted against time after stress change. The slope and the ordinate intercept yield the para-

meters in Equation (20).

Figure 6: Loading and unloading experimental data of grain matrix anelastic strain as a function of time after stress change. The uncertainty in the strain is of the order of 3×10^{-6}. The curves shown are calculated from Equation (21).

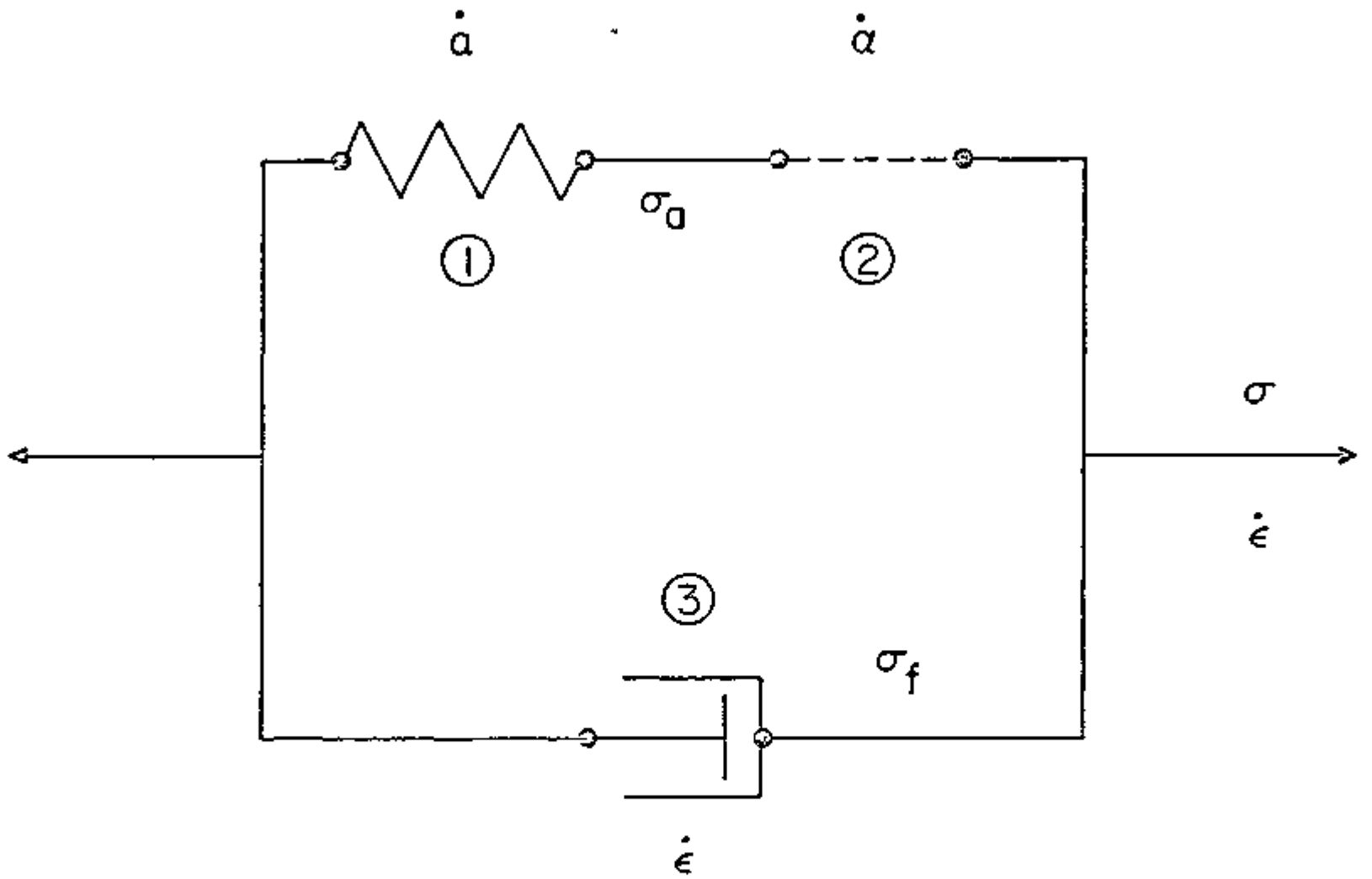
$\dot{a}$
$\dot{\alpha}$
σ_a
①
②
σ
$\dot{\epsilon}$
③
σ_f
$\dot{\epsilon}$

FIG. 1

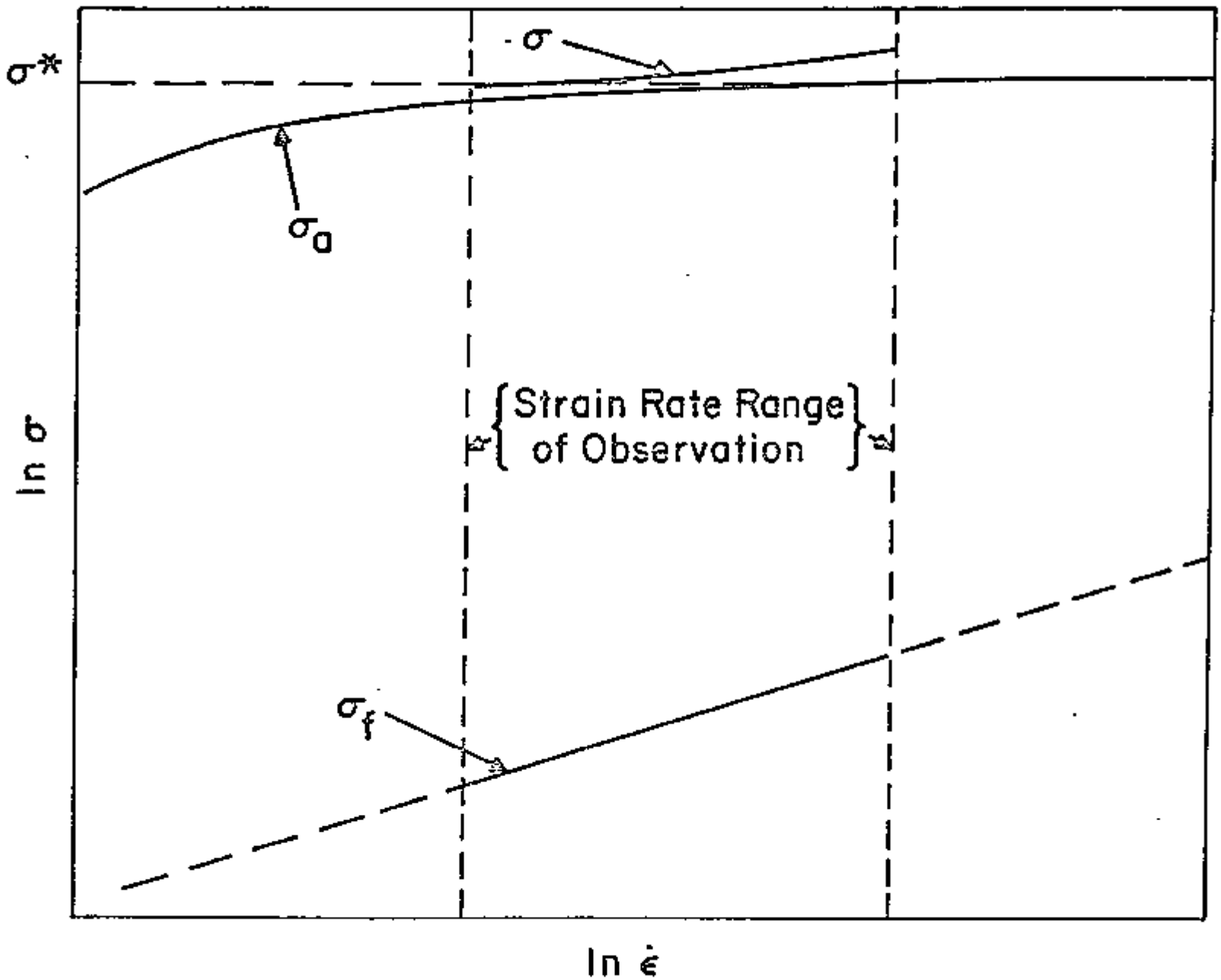

FIG. 2

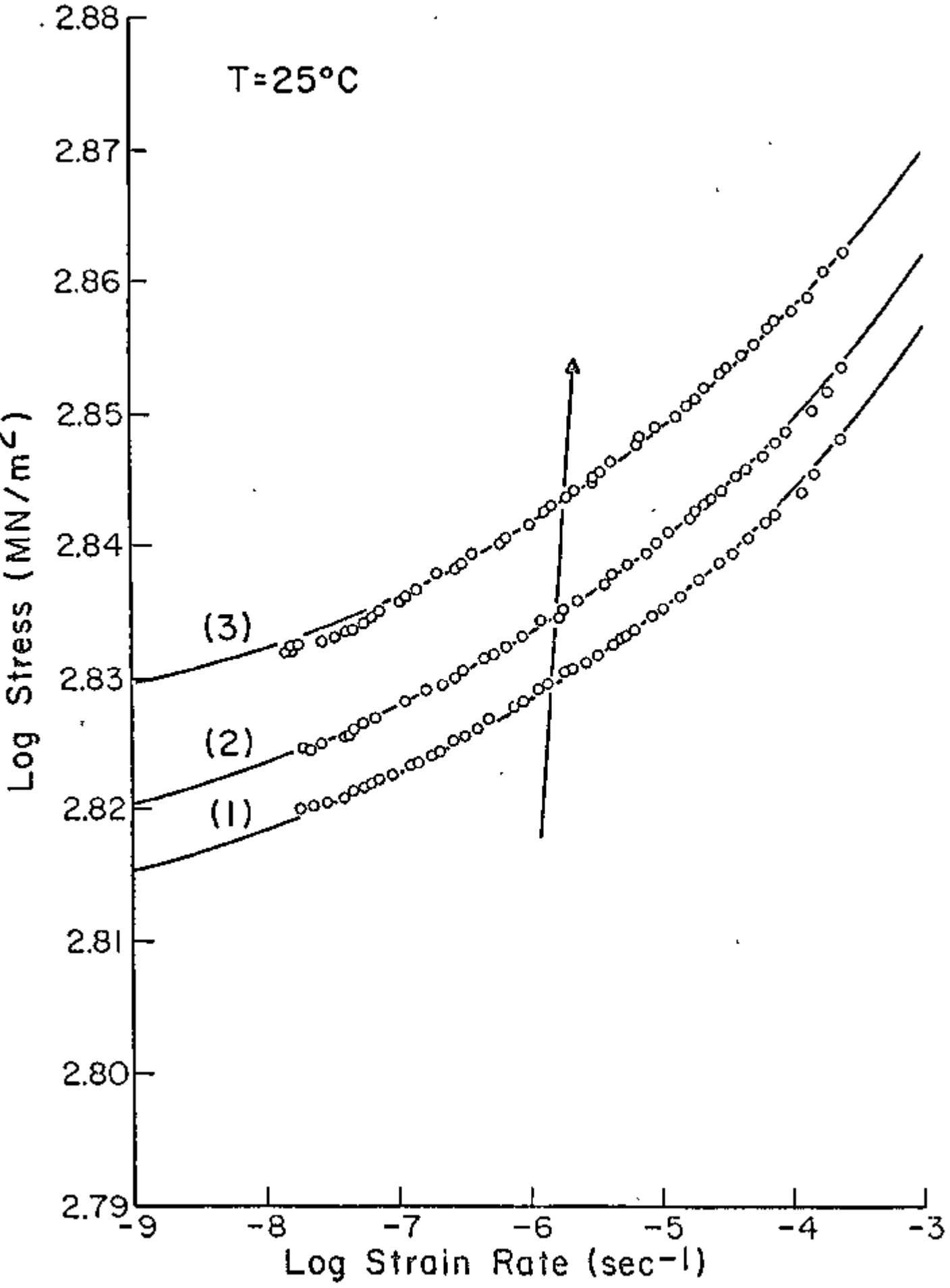
T=25°C
2.88
2.87
2.86
2.85
2.84
2.83
2.82
2.81
2.80
2.79
Log Stress (MN/m2)
(3)
(2)
(1)
-9
-8
-7
-6
-5
-4
-3
Log Strain Rate (sec-1)

FIG. 3

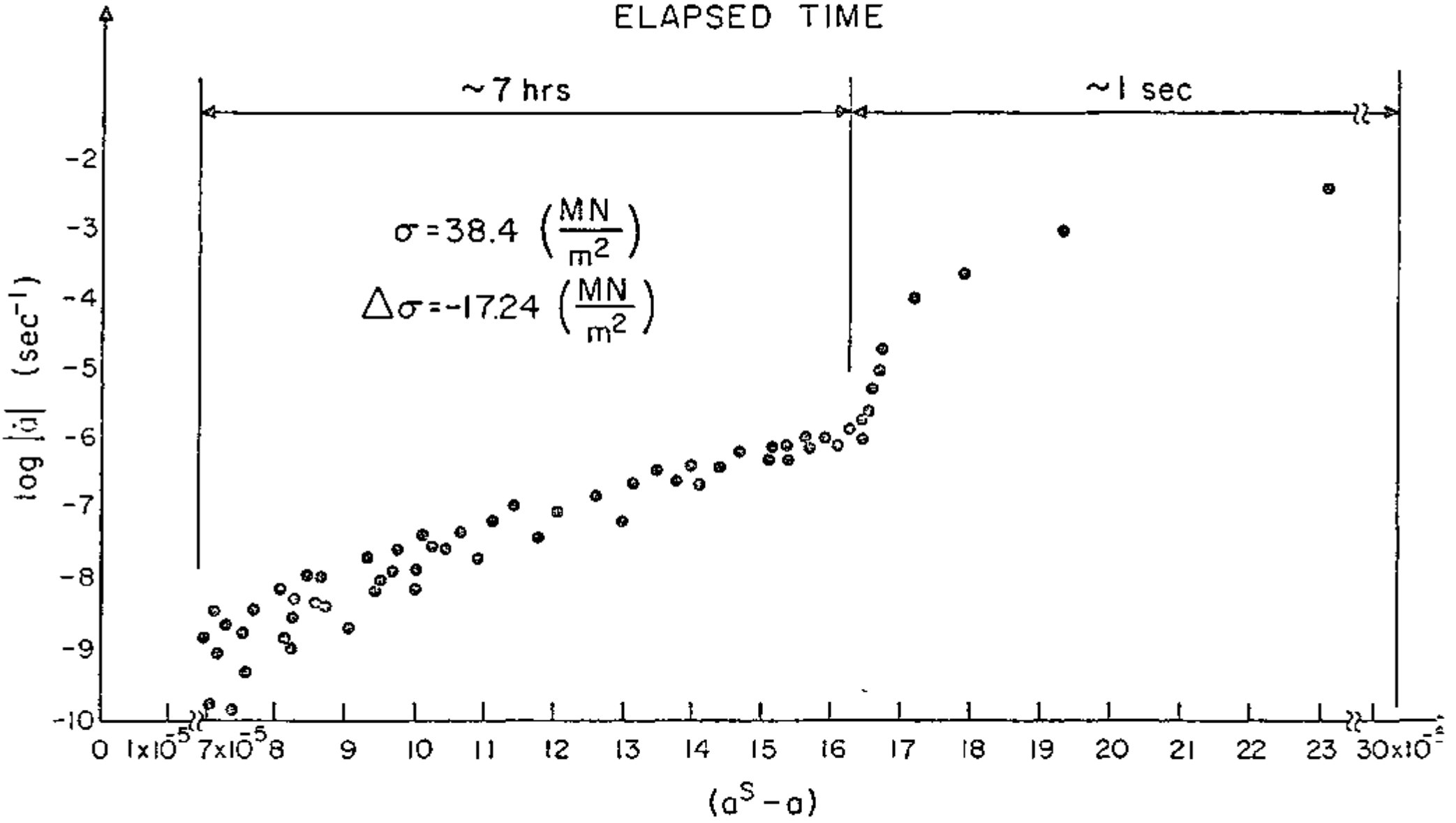
ELAPSED TIME
~7 hrs
~1 sec
$\sigma = 38.4 \left(\frac{MN}{m^2}\right)$
$\Delta\sigma = -17.24 \left(\frac{MN}{m^2}\right)$
log |$\dot{a}$| (sec^{-1})
-2
-3
-4
-5
-6
-7
-8
-9
-10
0
1x10^{-5}
7x10^{-5}
8
9
10
11
12
13
14
15
16
17
18
19
20
21
22
23
30x10^{-5}
$(a^S - a)$

FIG. 4

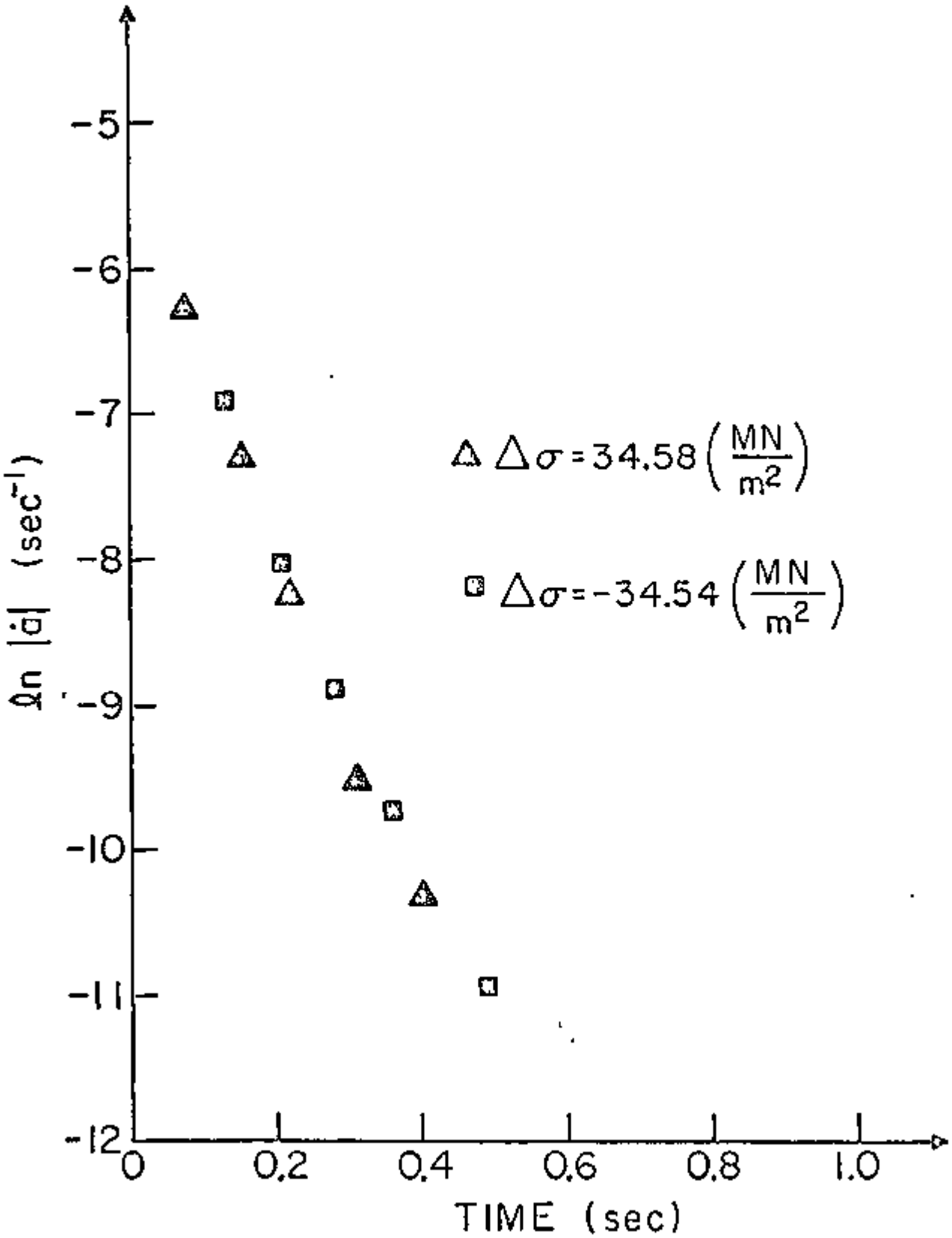
-5
-6
-7
-8
-9
-10
-11
-12
0
0.2
0.4
0.6
0.8
1.0
TIME (sec)
ℓn |ȧ| (sec⁻¹)
Δ Δσ = 34.58 (MN/m²)
□ Δσ = -34.54 (MN/m²)

FIG. 5

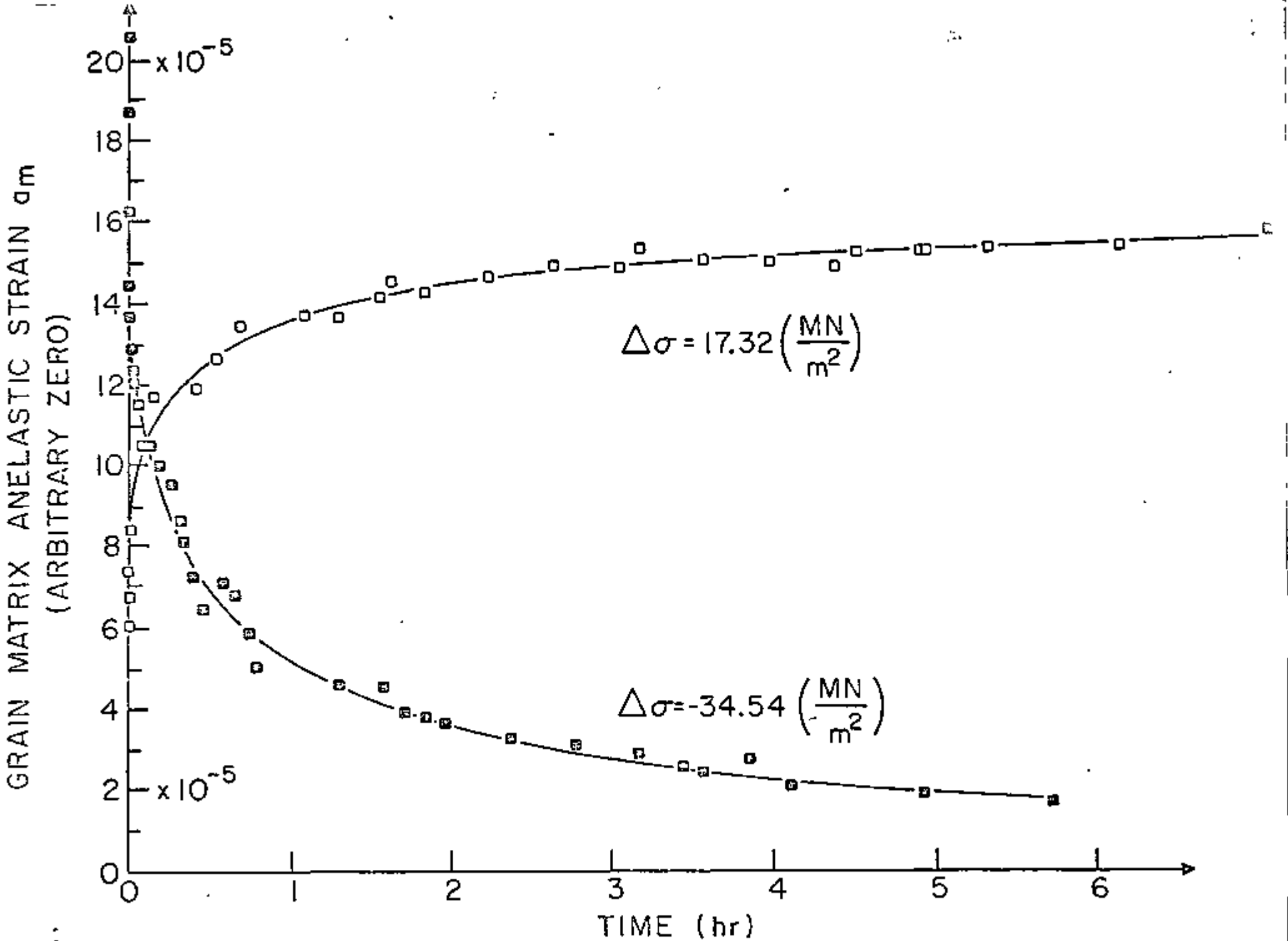
GRAIN MATRIX ANELASTIC STRAIN α_m
(ARBITRARY ZERO)
20 x 10⁻⁵
18
16
14
12
10
8
6
4
2
x 10⁻⁵
0
0
1
2
3
4
5
6
TIME (hr)
$\Delta\sigma = 17.32 \left(\frac{MN}{m^2}\right)$
$\Delta\sigma = -34.54 \left(\frac{MN}{m^2}\right)$

FIG. 5